INVESTIGATION OF FIRST ORDER PHASE TRANSITION PROCESS OF STRONIUM DURING HEATING WITH MOLECULAR DYNAMICS SIMULATIONS USING DIFFERENT POTENTIALS

Murat Celtek[1], Unal Domekeli[2], Sedat Sengul[2]

[1]Faculty of Education, Trakya University, 22030, Edirne – TURKEY
[2]Dept. of Physics, Trakya University, 22030, Edirne – TURKEY

Abstract

In the present study, the melting process of the face-centered cubic strontium (Sr) element, was investigated by classical molecular dynamics simulation. The embedded atom model and Morse potentials, which are from two different families, were used to describe the interactions between Sr atoms. The periodic boundary conditions were applied in all three directions of the simulation box containing 6912 atoms. All simulations were performed with the DL_POLY package program developed in the Daresbury laboratory. The first order phase (solid-liquid) transition during the heating process was monitored by using different analysis methods. The results obtained using both potential functions were discussed by comparing with each other and with other results in the literature.

Keywords: molecular dynamic simulations, solid-liquid phase, interatomic potentials, strontium, pair distribution function

INTRODUCTION

Strontium (Sr) is one of the most common elements in nature and is even the 15th most abundant element in the earth's crust. Consumption of Sr is usually in the form of strontium carbonate. It is commonly used in high-voltage television tubes in the form of carbonate. Sr is also used in the manufacture of ceramic ferrites, which are used in the automotive industry, iron ore separators, copiers and special alloys. Sr, which has a large atomic radius, is also used to neutralize x-rays. Apart from these, strontium sulfide is used in fireworks and paints; strontium nitrate is used in the pharmaceutical industry and in fireworks because it gives a deep red color to the flame; Strontium oxide is a compound also used in pharmaceuticals and is used as an intermediate in the production of strontium ferrite. Strontium hydroxide is a compound used in sugar mills to recover sugar from molasses. Strontium silicate compound, on the other hand, is an important ingredient in the production of high-quality iron [1]. Sr is also known as a bone trace element and has chemical similarity with calcium (Ca) element, so most researchers use it as a replacement ion for Ca in Hydroxyapatite (HAp) [2, 3]. It is accepted that partial substitution of Ca with Sr can improve the biological properties of HAp [4]. Moreover, it has been stated in some studies that the inclusion of Sr in HAp can increase the dissolution rate of HAp as well as increase the adsorption capacity of drugs [5]. In recent years, Sun et al. [6] have studied the effects of Sr incorporation into Mg-Zn-Ca biodegradable bulk metallic glass by both molecular dynamics (MD) simulation and density functional theory calculation. They observed that the results of the newly obtained Mg-Zn-Ca-Sr BMG were quite consistent with previously reported experimental results. The fact that its usage area is so wide and that it gives unique properties to the materials it is added to, increases the interest in Sr element and its alloys even more today. Thus, in the present study, we focused on the changes in the atomic structure of pure Sr during the heating process. To describe the interactions between Sr atoms in all MD simulations, we chose the embedded atom model (EAM) and Morse potentials, which are widely preferred in the literature. In the following sections, the

326

results obtained from the MD simulations will be discussed in detail using different analysis methods.

EXPOSITION

In classical MD simulations, EAM potentials are mostly preferred to describe pairwise interactions in metals and metal alloys. According to this approximation, the total energy E_i of the i atoms is given as:

$$E_i = F_\alpha\left[\sum_{j\neq i}\rho_{\alpha\beta}\left(r_{ij}\right)\right] + \frac{1}{2}\sum_{j\neq i}\phi_{\alpha\beta}\left(r_{ij}\right) \qquad (1)$$

where α and β are the element types of atoms i and j. F_α is the embedding energy that is expressed as a function of atomic electron density (ρ). $\phi_{\alpha\beta}(r_{ij})$ is the pair interaction energy between i and j atoms separated at a distance of r_{ij} from each other. The EAM potential data used in the present study were taken from Sheng [7] who reproduced and shared it into literature. Another energetic function used here is the Morse pair potential, which is widely preferred in MD simulations. The energy function of the Morse potential is given as:

$$\phi(r) = D_0\left(e^{-2\alpha\left(r_{ij}-r_0\right)} - e^{-\alpha\left(r_{ij}-r_0\right)}\right) \qquad (2)$$

where r_{ij} is the distance between i and j atoms, r_0 is the equilibrium bond length, D_0 is the potential well depth. α is a parameter that controls the width of the potential. Morse potential parameters for pure Sr are given in Table 1 [8].

Table 1. Morse potential parameters used for pure Sr.

	D_0 (eV)	α (Å⁻¹)	r_0 (Å)
Sr-Sr	0.1513	0.73776	4.988

All simulations were performed with the DL_POLY 2.0 package program developed by Smith et al. [9] at Daresbury laboratories and offered as open source. Initially, the system was formed in the face-centered cubic (FCC) structure, which is the most stable structure for solid Sr. The periodic boundary conditions were applied in all three main axes of FCC crystal structure containing 4 atoms in the unit cell and the total number of atoms in the MD simulation cell was determined to be 6912 (4x(12x12x12)). The velocity form of Verlet algorithm was used to solve Newton's motion equations. The temperature and pressure were controlled by the Berendsen thermostat and barostat throughout the simulations. The system was heated the starting from 0 K up to 1600 K (with 50 K increments), a temperature well above the melting point of Sr (T_m = 1042 K [10], 1050 K [11]), using the isothermal-isobaric (NPT) ensemble and the time step of 1 fs. The temperature-dependent changes of the energy per atom during the heating process for the EAM and Morse potentials are shown in Fig. 1. While the calculated energies values for Morse and EAM potentials change almost linearly up to 600 K and 1100 K, respectively, a sudden change is observed at these points. This shows that the system passes from solid to liquid phase by making a first-order phase transition at 600 K for Morse potential and 1100 K for EAM potential. These results show that the Morse potential predicts the melting point of Sr with a deviation of -52.02% and the EAM potential with a deviation of +5.57% when compared with the experimental melting point given in Ref [10]. The present findings show that the EAM potential predicts the melting point of Sr quite successfully when compared to the Morse potential. The cohesive energies for EAM and Morse potential were determined as -1.72 eV/atom and -1.08 eV/atom, respectively, which shows that the EAM potential results are in good agreement with the experimental value (-1.72 eV/atom [10]) in the literature. In addition, the snapshots of the simulation box at 50 K, 1100 K, and 1150 K are given in the inset of the figure (only for EAM potential). As in crystal-like structures, while Sr atoms have an ordered structure at 50 K, this order disappears at the melting point at 1100 K with increasing temperature, and the structure takes on a form in which both the crystal and liquid phases coexist. When the temperature rises to 1150 K, all the atoms in the box become completely disordered, which is a clear indication that the system is now liquid.
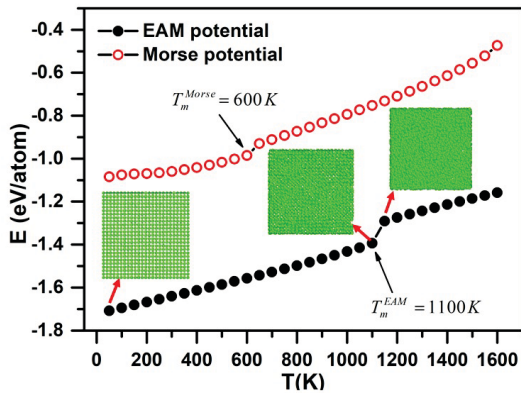
Fig. 1. *Evolution of energy per atom as a function of temperature during the heating process.*

The temperature-dependent variation of the lattice parameters determined during the heating process for both potentials are shown in Fig. 2 together with the experimental value [10]. As expected, the lattice parameters determined for both potentials increase with increasing temperature, and a sudden increase is observed around the melting point, just like in the energy-temperature curves. The lattice parameter determined for the EAM potential is quite consistent with the experimental value, and the Morse potential produces much larger values than the experimental value. The values calculated and discussed up to this section are indispensable for successful MD simulations of a material. In other words, an interatomic potential that cannot predict these values well will fail to predict the physical properties of the material and the results it produces cannot be trusted. According to the results available so far, Morse potentials are not very successful in determining the structural and other properties of Sr. Contrary to Morse potential, EAM has been quite successful in explaining many properties of Sr.
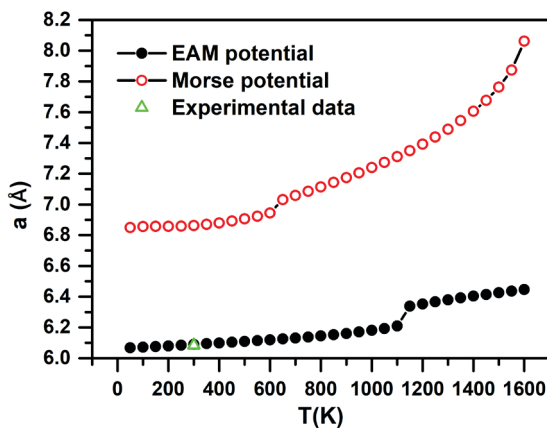
Fig. 2. *Lattice parameters as a function of temperature for both potentials. Experimental data are taken from Ref [10].*

The pair distribution function, $g(r)$, represents the probability of finding another atom at a distance r from a reference atom. $g(r)$ (or structure factor $S(q)$) curves are frequently used to determine phase transitions during heating and cooling processes, as well as to characterize the structural properties of solid, liquid, and amorphous systems [12–16] The expression of $g(r)$ used in the MD simulation is as follows;

$$g(r) = \frac{V}{N^2} \left\langle \sum_i^N \sum_{j \neq i}^N \delta(r - r_{ij}) \right\rangle \qquad (3)$$

where V and N represent the volume of the simulation box and the number of atoms in the box, respectively. $S(q)$ is obtained from the Fourier transform of $g(r)$ as follows;

$$S(q) = 1 + 4\pi\rho \int_0^\infty r^2 \frac{\sin qr}{qr} (g(r) - 1) dr \qquad (4)$$

where ρ is the average number density. The $g(r)$ curves calculated for both potentials at different temperatures are given together in Fig. 3. There are differences in the positions of the main peaks of $g(r)$'s obtained at 300 K for both potentials, but they produce sharp main peaks, which are characteristic of FCC crystal structure. At 500 K, although the main peak of $g(r)$ for the EAM potential soften slightly, $g(r)$ still has very prominent FCC peaks, whereas for the Morse potential the main peak of $g(r)$ decreases significantly at this temperature, which is attributed to the fact that the system contains complex structures together. With the increase in temperature, the $g(r)$ curves calculated for the Morse potential at temperatures of 700 K and above exhibit softer and larger amplitude peaks reflecting the characteristic of liquid structures. On the other hand, the sharp peaks still seem to be dominant for the EAM potential. The heights of these peaks decrease and the width of them increase with increasing temperature. Finally, when the temperature is increased to 1300 K, the $g(r)$ curve calculated for the EAM potential now shows a peaks specific to liquid state, and this behavior is a clear signature of the melting of the system.
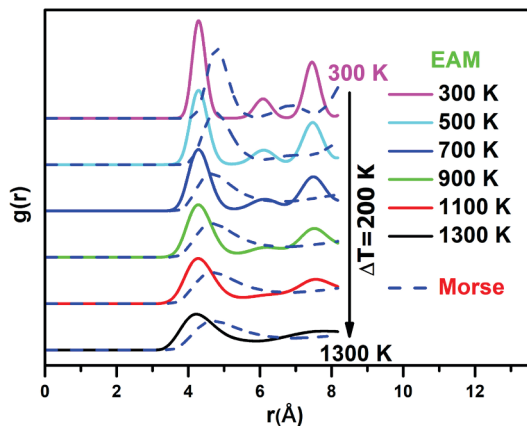
Fig. 3. *Comparison of simulated g(r)'s at different temperatures for EAM and Morse potentials.*

The *g(r)* and *S(q)* curves calculated for the EAM (at 1150 K) and Morse (at 1050 K) potentials of liquid Sr are plotted in Fig. 4 together with the experimental data reported by Waseda (1053 K) [17]. While both the *g(r)* and *S(q)* curves calculated for the EAM potential are in good agreement with the experimental data, the positions and heights of their peaks for the Morse potential are very different from the experimental data. The consistency between the EAM-MD simulations and the experimental data indicates that the EAM potential can accurately describe the interactions between Sr atoms in the system and predict the positions of the atoms. Morse potential, on the other hand, gives unsuccessful results for Sr and cannot accurately describe the physical properties of Sr by MD simulation method, so it is recommended to reconsider the potential parameters. At the same time, these results also support the results discussed above.
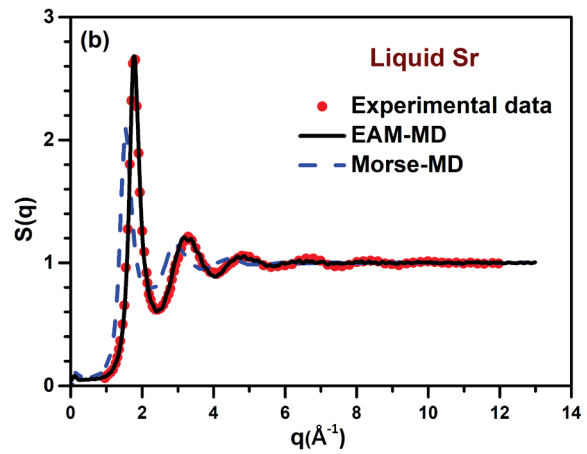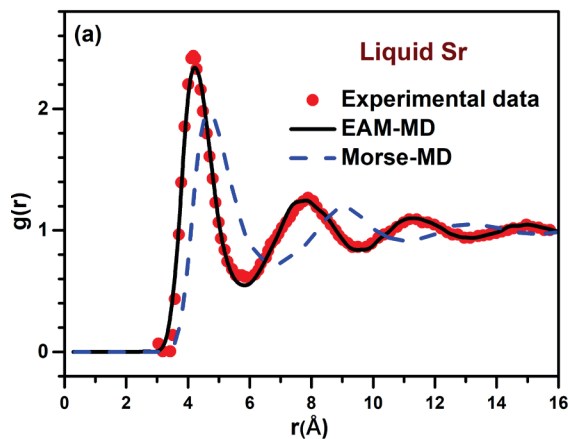
Fig. 4. *Calculated (a) g(r) and (b) S(q) curves for EAM (at 1150 K) and Morse (at 1050 K) potentials of liquid Sr. Experimental data have been taken from Waseda (at 1053 K) [17].*

In our study, we obtained information about the evolution of the microstructure of the system throughout the heating process, using the Honeycutt-Andersen (HA) index analysis method to describe the process well [18]. In the HA technique, four different integer index sequences, *ijkl*, are used to characterize the local environment of bonded pairs. The first integer *i* indicates whether the two given atoms are bonded. That is, the first integer is 1 if the root pairs are bonded, 2 otherwise. The second integer *j* represents the number of nearest neighbor atoms in common with pairs of roots. The third integer *k* gives the number of nearest neighbor bonds between these common points. If the fourth integer is *l*, it is a parameter used to distinguish local structures when the first three integers *(i, j, k)* are the same. According to this technique, 1431 and 1541 bonded pairs are characteristic of defective icosahedra, while 1551 bonded pairs are characteristic of icosahedra order. 1421 and 1422 bonded pairs are characteristic of FCC and hexagonal close-packed (HCP) crystal structures, respectively. Finally, the 1661 and 1441 bonded pairs are characteristic of the body-centered cubic (BCC) crystal structure. The schematic representation of the most common bonded pairs mentioned is given in Fig. 5.
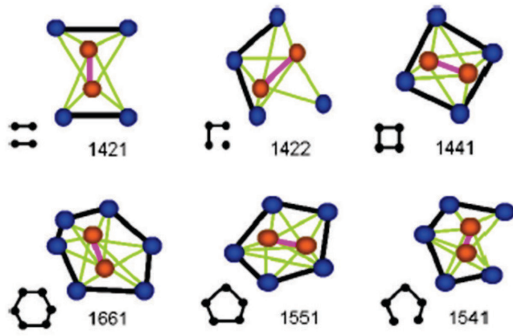
Fig. 4. *Display of some of the most common bonded pairs* [19].

With the HA method applied to the data obtained from the EAM-MD and Morse-MD simulations, the most common bonded pairs (1421, 1422, 1661, 1441, 1551, 1541 and 1431) in the system have been determined and their temperature-dependent evolutions are presented in Fig. 5. This figure also represents the temperature-dependent microstructure changes during the first-order phase transition. In Fig. 5, the percentage of 1421 bonded pairs found at low temperatures has been 100% for both potentials. Since the 1421 bonded pairs represent the FCC structure, this indicates that the system is stable in the FCC crystal structure. The percentage of these bonded pairs decreases with increasing temperature, with a sharp decrease around the melting point for each potential, dropping to almost 0%. Meanwhile, a certain increase is observed in other bonded pairs depending on the increasing temperature. Of particular interest is the increase of 1541 bonded pairs representing defective FCC clusters. This means that 1421 bonded pairs start to deteriorate with the effect of temperature and they are replaced by 1541 bonded pairs. These results show that there are significant changes in the structure of Sr during the heating. In other words, 1421 bonded pairs representing the natural structure of the system, turn into 1431 and 1541 bonded pairs and other bonded pairs with increasing temperature. In terms of HA analysis results, it has been observed that the system maintains its stable structure during the heating process at both potentials.
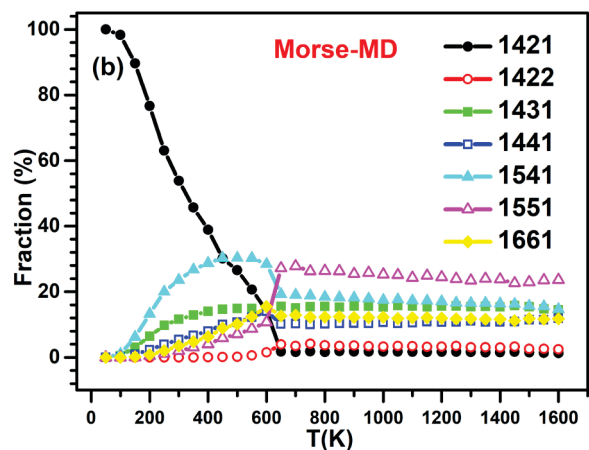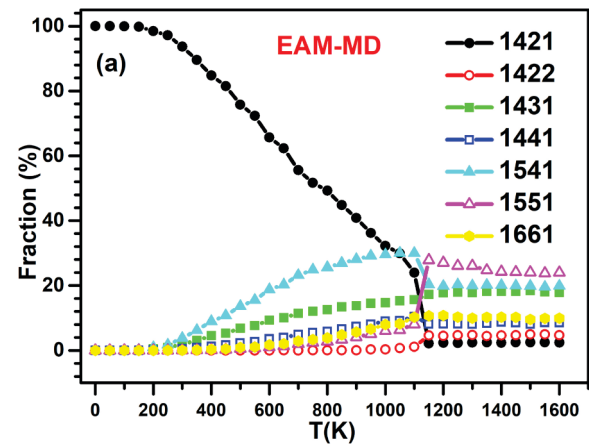
Fig. 5. *Temperature-dependent variation of the most dominant bonded pairs according to HA analysis of (a) EAM-MD and (b)Morse-MD simulation results.*

CONCLUSION

In this study, EAM and Morse potentials were used to investigate the effect of potential functions on some physical properties of FCC Sr such as structural evolution and melting point with the help of MD simulation method. While the EAM potential is successful in explaining all the physical properties of Sr calculated in this study, the Morse potential cannot respond to the demands. This once again reveals how important the selected potential in MD simulations is. A review of Morse potential parameters for Sr is recommended, and it is thought that the results of the current study will encourage scientists to examine the dynamic, mechanical properties and behavior of Sr under pressure.

REFERENCE

[1]   Eskier U. What is Strontium and Where Is It Used?,
https://www.makaleler.com/stronsiyum-nedir (2021).

[2]   Chadha RK, Singh AP, Singh KL, vd. Influence of microwave processing and sintering temperature on the structure and properties of Sr/Zr doped hydroxyapatite. Mater Chem Phys 2019; 223: 319–324.

[3]   Yan S, Xia P, Xu S, vd. Nanocomposite Porous Microcarriers Based on Strontium-Substituted HA- g -Poly(γ-benzyl- l -glutamate) for Bone Tissue Engineering. ACS Appl Mater Interfaces 2018; 10: 16270–16281.

[4]   Park SY, Kim K-I, Park SP, vd. Aspartic Acid-Assisted Synthesis of Multifunctional Strontium-Substituted Hydroxyapatite Microspheres. Cryst Growth Des 2016; 16: 4318–4326.

[5]   Zhu H, Guo D, Sun L, vd. Nanostructural insights into the dissolution behavior of Sr-doped hydroxyapatite. J Eur Ceram Soc 2018; 38: 5554–5562.

[6]   Sun S-J, Ju S-P, Yang C-C, vd. Effects of Strontium incorporation to Mg-Zn-Ca biodegradable bulk metallic glass investigated by molecular dynamics simulation and density functional theory calculation. Sci Rep 2020; 10: 2515.

[7]   Sheng H. EAM potentials, https://sites.google.com/site/eampotentials/Sr (2021).

[8]   Girifalco LA, Weizer VG. Application of the Morse Potential Function to Cubic etals. Phys Rev 1959; 114: 687–690.

[9]   Smith W, Forester TR. DL_POLY_2.0: A general-purpose parallel molecular dynamics simulation package. J Mol Graph 1996; 14: 136–141.

[10]   Kittel C. *Introduction to Solid State Physics*. New York: John Wiley & Sons Inc., 1986.

[11]   The periodic table of the elements, http://www.webelements.com/strontium/crystal_structure.html (2021).

[12]   Sengul S, Celtek M. Pressure Effects on the Structural Evolution of Monatomic Metallic Liquid Hafnium. BEU J Sci 2018; 7: 144–158.

[13]   Celtek M. The effect of atomic concentration on the structural evolution of Zr100-xCox alloys during rapid solidification process. J Non Cryst Solids 2019; 513: 84–96.

[14]   Celtek M, Sengül S. Effects of cooling rate on the atomic structure and glass formation process of Co90Zr10 metallic glass investigated by molecular dynamics simulations. Turkish J Phys 2019; 43: 11–25.

[15]   Sengul S, Celtek M, Domekeli U. The structural evolution and abnormal bonding ways of the Zr80Pt20 metallic liquid during rapid solidification under high pressure. Comput Mater Sci 2020; 172: 109327.

[16]   Celtek M, Sengul S, Domekeli U, vd. Dynamical and structural properties of metallic liquid and glass Zr48Cu36Ag8Al8 alloy studied by molecular dynamics simulation. J Non Cryst Solids 2021; 566: 120890.

[17]   Waseda Y. *The Structure of Non-Crystalline Materials-Liquids and Amorphous Solids*. New York: London: McGraw-Hill, 1981.

[18]   Honeycutt JD, Andersen HC. Molecular Dynamics Study of Melting and Freezing of Small Lennard- Jones Clusters. J Phys Chem 1987; 91: 4950–4963.

[19]   Çelik FA. CuAu ve Cu3Au Süper Alaşımların Bazı Termal Özelliklerinin Moleküler Dinamik Çalışması. J Inst Sci Technol 2021; 11: 1939–1947.